

## RESEARCH ARTICLE

10.1002/2017JD027015

## Key Points:

- We develop a new method for comparing a chemistry-climate model to satellite observations of in-cloud ozone
- A CCM captures major features of the in-cloud ozone distribution
- Convection reduces ozone at 400 hPa over most of the tropics but increases it over highly polluted regions in South and East Asia

## Supporting Information:

- Supporting Information S1

## Correspondence to:

S. A. Strode,  
sarah.a.strode@nasa.gov

## Citation:

Strode, S. A., Douglass, A. R., Ziemke, J. R., Manyin, M., Nielsen, J. E., & Oman, L. D. (2017). A model and satellite-based analysis of the tropospheric ozone distribution in clear versus convectively cloudy conditions. *Journal of Geophysical Research: Atmospheres*, 122, 11,948–11,960. <https://doi.org/10.1002/2017JD027015>


Received 27 APR 2017

Accepted 16 OCT 2017

Accepted article online 20 OCT 2017

Published online 7 NOV 2017

# A Model and Satellite-Based Analysis of the Tropospheric Ozone Distribution in Clear Versus Convectively Cloudy Conditions

Sarah A. Strode<sup>1,2</sup> , Anne R. Douglass<sup>2</sup> , Jerald R. Ziemke<sup>2,3</sup>, Michael Manyin<sup>2,4</sup>, J. Eric Nielsen<sup>2,4</sup> , and Luke D. Oman<sup>2</sup> 

<sup>1</sup>Universities Space Research Association, Columbia, MD, USA, <sup>2</sup>NASA Goddard Space Flight Center, Greenbelt, MD, USA, <sup>3</sup>Morgan State University, Baltimore, MD, USA, <sup>4</sup>Science Systems and Applications, Inc., Lanham, MD, USA

**Abstract** Satellite observations of in-cloud ozone concentrations from the Ozone Monitoring Instrument and Microwave Limb Sounder instruments show substantial differences from background ozone concentrations. We develop a method for comparing a free-running chemistry-climate model (CCM) to in-cloud and background ozone observations using a simple criterion based on cloud fraction to separate cloudy and clear-sky days. We demonstrate that the CCM simulates key features of the in-cloud versus background ozone differences and of the geographic distribution of in-cloud ozone. Since the agreement is not dependent on matching the meteorological conditions of a specific day, this is a promising method for diagnosing how accurately CCMs represent the relationships between ozone and clouds, including the lower ozone concentrations shown by in-cloud satellite observations. Since clouds are associated with convection as well as changes in chemistry, we diagnose the tendency of tropical ozone at 400 hPa due to chemistry, convection and turbulence, and large-scale dynamics. While convection acts to reduce ozone concentrations at 400 hPa throughout much of the tropics, it has the opposite effect over highly polluted regions of South and East Asia.

## 1. Introduction

Deep convection strongly impacts the tropospheric ozone distribution by vertically redistributing ozone and its precursors (Gidel, 1983; Lelieveld & Crutzen, 1994). Analysis of satellite observations suggests that convection drives much of the large-scale variability in tropospheric ozone over the Pacific (Ziemke et al., 2015). Convection over polluted regions enhances chemical production of ozone (Pickering et al., 1992; Thompson et al., 1997), and observations show that ozone concentrations increase with time since convection occurred (Bertram et al., 2007). Clouds impact the chemistry by changing UV fluxes (Wang & Prinn, 2000) and photolysis rates. Clouds alter the vertical profile of photolysis rates, increasing photolysis rates above the cloud and decreasing them below (Liu et al., 2006; Voulgarakis et al., 2009). Heterogeneous chemistry in cloud droplets can also affect ozone concentrations (Jacob, 2000, and references therein). Furthermore, convection is often accompanied by lightning emissions of NO<sub>x</sub>, contributing to ozone formation. Additionally, observations from the DC3 campaign show that convective overshooting leads to the transport of high ozone air from the stratosphere into the anvil outflow in the upper troposphere (Huntrieser et al., 2016).

On the other hand, the upper troposphere of the southwest tropical Pacific shows low ozone values due to the presence of deep convection (Kley et al., 1996; Solomon et al., 2005). By lofting air containing low ozone concentrations, convection opposes the tendencies of downward vertical advection and chemistry to increase ozone (Folkens et al., 2002). A global modeling study by Lawrence et al. (2003) found that while convective transport of ozone leads to higher ozone concentrations at the surface, thus increasing the loss by deposition, this effect is outweighed by the increased ozone production due to convective transport of ozone precursors.

Ozone profiles from sondes launched in the tropics typically exhibit an S shape, with a minimum above 11 km associated with convective outflow (Folkens et al., 2002; Thompson et al., 2011). Alternatively, Pan et al. (2015) interpret the S shape as the result of averaging two modes, with convective mixing of near-surface ozone values forming the primary mode.

The combined effects of deep convection over the Pacific and Indian Oceans, and downwelling over the Atlantic along with biomass burning over Africa, lead to the wave-one pattern of higher ozone over Africa and the Atlantic than over the Pacific seen in satellite observations and ozonesondes (Fishman & Larsen, 1987; Thompson et al., 2003). The pattern of lower ozone over the tropical Pacific compared to the Atlantic is also evident in the tropospheric ozone column derived from a combination of Aura Ozone Monitoring Instrument (OMI) and Microwave Limb Sounder (MLS) data (Ziemke et al., 2006; Ziemke et al., 2011).

OMI/MLS observations of ozone inside deep convective clouds (Ziemke et al., 2009) provide global information on the influence of convection on upper tropospheric ozone concentrations. Upper tropospheric ozone concentrations are especially important since the radiative forcing efficiency of ozone in the upper troposphere exceeds that of the lower troposphere (Lacis, Wuebbles, & Logan, 1990).

The OMI/MLS in-cloud ozone product provides an opportunity to test how well chemistry-climate models (CCMs) reproduce the relationship between clouds, convection, and upper tropospheric ozone throughout the tropics. However, the comparison is not straightforward since clouds in a free-running CCM will not exactly match the observed clouds in space and time, and the spatial resolution of a CCM is typically large enough to include both clear and cloudy fractions within a grid box. Here we develop a method for comparing in-cloud ozone in a CCM to the OMI/MLS in-cloud product. We then use the CCM to quantify the contributions of large-scale dynamics, convection and turbulence, and chemistry to the ozone distribution.

## 2. Methods

### 2.1. OMI/MLS Observations

The OMI and MLS instruments on the NASA Aura satellite provide data on the above-cloud and stratospheric ozone columns, respectively. Ziemke et al. (2009) and Ziemke et al. (2017) describe a method for calculating the ozone inside tropical deep convective clouds based on the OMI/MLS residual. We summarize the method briefly here. The OMI measured ozone column includes ozone between the top of the atmosphere and the optical centroid pressure (OCP). The OCP is the characteristic pressure of a single cloud layer retrieved by OMI (Joiner et al., 2012) and is set to match the observed rotational-Raman scattering signal (Stammes et al., 2008). We refer the reader to Vasilkov et al. (2008) and Ziemke et al. (2017) for a detailed discussion. Since UV radiation from the Sun can penetrate deeply into thick clouds, Vasilkov et al. (2008) found that the OCP is typically located at a pressure several hundred hectopascal greater than the cloud top. Consequently, subtracting the MLS stratospheric column ozone from the OMI ozone column provides the in-cloud ozone, defined as the average ozone concentration between the OCP and the tropopause. The column difference is converted from Dobson units to volume mixing ratio (ppmv) using the following equation (Joiner et al., 2009; Ziemke, Chandra, & Bhartia, 2001):

$$X = 1,270^* \Delta\Omega / (P_{\text{eff}} - P_{\text{trop}})$$

where  $X$  is the average volume mixing ratio,  $\Delta\Omega$  is the column ozone difference,  $P_{\text{eff}}$  is the effective scene pressure, and  $P_{\text{trop}}$  is the tropopause pressure. This method assumes that the cloud top is near the tropopause, as the in-cloud ozone definition will include ozone that lies between the cloud top and the tropopause.

Ziemke et al. (2009) created monthly gridded fields of in-cloud ozone based on OMI pixels with reflectivity over 80% and OCP values between 250 and 550 hPa to select only upper tropospheric ozone in deep convective clouds. Our study uses both the in-cloud ozone and the background (reflectivity less than 30%) ozone from the OMI/MLS residual method (Ziemke et al., 2006). The in-cloud ozone dataset has now been extended to multiple years, as described in Ziemke et al. (2017). We use the data from 2005 through 2014.

### 2.2. Chemistry-Climate Model Simulations

We use a multiyear simulation of the Goddard Earth Observing System version 5 (GEOS-5) Chemistry-Climate Model (GEOSCCM) for comparison with the OMI/MLS in-cloud and background ozone. Molod et al. (2015) summarizes the GEOS-5 physical parameterizations. Briefly, GEOS-5 uses the Relaxed Arakawa-Schubert scheme (Moorthi & Suarez, 1992) to parameterize convection. The cloud water and ice scheme as well as the prognostic cloud cover are described by Bacmeister, Suarez, and Robertson (2006). Turbulent mixing is parameterized based on Helfand and Schubert (1995) for the surface layer and based on Lock et al. (2000) and Louis and Geleyn (1982) above the surface layer.

The GEOSCCM (Oman et al., 2011; Pawson et al., 2008) uses the Global Modeling Initiative (GMI) chemistry mechanism (Duncan et al., 2007; Strahan, Duncan, & Hoor, 2007) to simulate ozone and other trace gases within the GEOS-5 atmospheric general circulation model. The GMI mechanism includes over 400 reactions to represent stratospheric and tropospheric chemistry, including the interactions between  $\text{NO}_x$ , hydrocarbons, and ozone. Aerosols are simulated by the Goddard Chemistry Aerosol Radiation and Transport component of GEOS-5 (Chin et al., 2002; Colarco et al., 2010) and interact with the GMI chemistry. GEOS-5 also includes an idealized methyl iodide ( $\text{CH}_3\text{I}$ ) tracer, which has a uniform source at the surface over water only and is lost throughout the atmosphere with a 5 day e-folding time. Since the flux is prescribed as a uniform value, we scale the resulting concentrations such that the mean surface concentration is 1 ppt.

We use the 2000–2010 period of the Ref-C1 GEOSCCM simulation conducted as part of the Chemistry-Climate Model Initiative (CCMI) (Eyring et al., 2013; Morgenstern et al., 2017). This simulation uses the Heracles version of GEOS-5 with 72 vertical levels and C48 horizontal resolution (cubed sphere, approximately  $2^\circ$ ), with the output remapped to a  $2^\circ$  by  $2.5^\circ$  latitude/longitude grid. The model is driven by observed sea ice distributions and sea surface temperatures from (Rayner et al., 2003). Anthropogenic and biomass burning emissions come from the MACCity inventory (Granier et al., 2011), which includes monthly and year-to-year variability. Lightning emissions are parameterized as described in Liaskos, Allen, and Pickering (2015). The simulation outputs the tendency of ozone due to different processes in the model including chemistry, convection, and large-scale transport.

GEOSCCM captures much of the observed response of tropospheric ozone to El Niño–Southern Oscillation (Oman et al., 2013). In the Atmospheric Chemistry and Climate Model Intercomparison Project (Lamarque et al., 2013), GEOSCCM showed good agreement with the outgoing longwave radiation from tropospheric ozone from the Tropospheric Emission Spectrometer (Bowman et al., 2013), suggesting that the ozone distribution is reasonable. Molod et al. (2015) presents an evaluation of GEOS-5 clouds. The simulated cloud fraction reproduces major features of the Atmospheric Infrared Sounder observations but overestimates the cloud fraction in the tropical upper troposphere.

### 2.3. Selection of Clear Versus Cloudy Days

We sort the daily CCM output into clear and cloudy categories for comparison to the background and in-cloud OMI/MLS data, respectively. As noted above, the OMI/MLS data are considered to be from deep convective clouds when reflectivity exceeds 80% and the OCP lies between 250 and 550 hPa. However, OCP is not a commonly available diagnostic from CCMs. While it would be possible to use an OMI simulator (Joiner et al., 2012) to calculate a grid column average OCP for the model, we instead choose an alternative definition based on cloud fraction for determining cloudiness in the model, as this is a readily available diagnostic requested by intercomparison studies such as CCMI. OMI data show a strong relationship between radiative cloud fraction and reflectivity, as shown in Figure S1 in the supporting information. Furthermore, since a two-degree model gridbox typically contains clear as well as cloudy regions over the course of a day, we need to apply cloud criteria to the model that retains grid columns that are not entirely cloudy.

We use the maximum cloud fraction between 350 and 400 hPa to categorize each grid column as cloudy or clear for a given day. The 350–400 hPa level is chosen to select for deep clouds and to avoid any biases in the simulation of high clouds. This simulated cloud fraction in the tropics is spatially correlated with both the model simulated planetary albedo ( $r = 0.78$  for the January mean and  $r = 0.85$  for the July mean) and the OMI reflectivity ( $r = 0.68$  for the January mean and  $r = 0.66$  for the July mean). We treat a grid column as cloudy if the 350–400 hPa cloud fraction equals or exceeds 0.4, and clear if it is less than that. We find that this threshold retains enough data to give the simulation results comparable spatial coverage to the OMI/MLS data, while requiring that a cloudy grid box includes a substantial portion of clouds. We sample the simulated ozone at 2 p.m. local time, consistent with the OMI overpass time.

## 3. Results

### 3.1. Evaluation of Simulated Tropospheric Ozone

Lang et al. (2012) evaluated tropospheric ozone from an earlier version of GEOSCCM against ozonesondes and tropospheric column ozone (TCO) from OMI/MLS (Ziemke et al., 2006). They found good agreement overall but a high bias in the simulated ozone for the middle and high latitudes of the Northern Hemisphere. Here

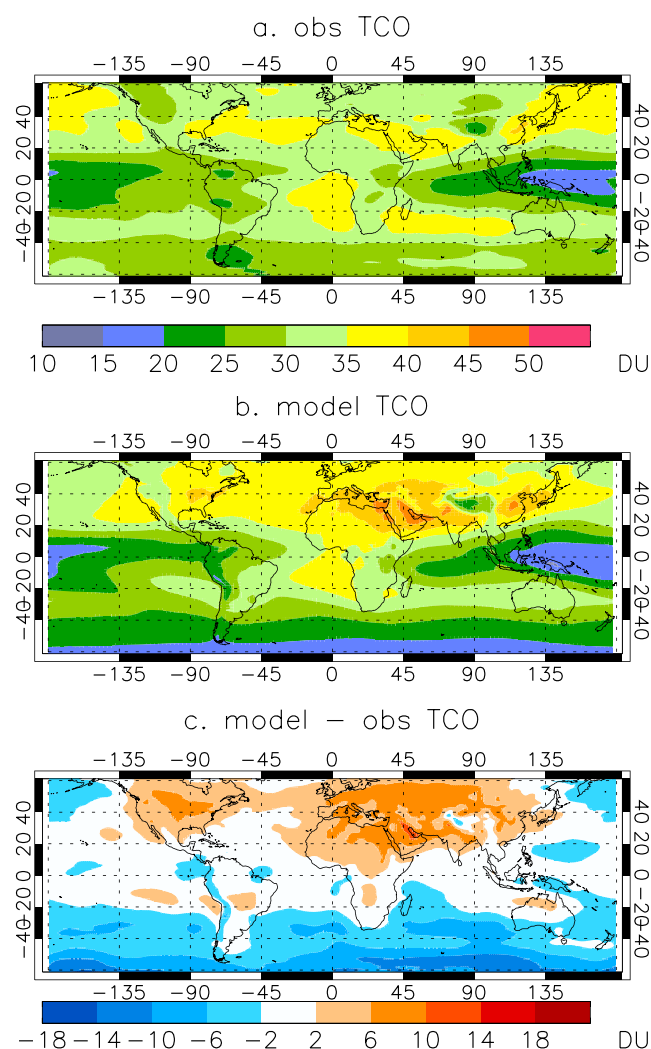


**Figure 1.** The tropospheric ozone column from (a) OMI/MLS climatology averaged from October 2004 to January 2011 and (b) the model simulation averaged over 2000–2010. (c) The difference between the simulated and OMI/MLS TCO.

we compare our simulation with a more recent model version that includes updates to the photolysis code, to the MLS/OMI climatology of Ziemke et al. (2011) in Figure 1. We find that the simulated TCO is biased high compared to OMI/MLS over the midlatitude continents, although this high bias is smaller than that found in Lang et al. (2012), and biased low over the southern oceans. However, the simulated TCO agrees well with OMI/MLS over much of the tropics. Differences in tropopause definition between the model and satellite product may also contribute to the TCO differences, particularly outside the tropics (Stajner et al., 2008).

Figure 2 shows a comparison of simulated ozone profiles to ozone sondes in the tropics for July. The ozone sonde data are from the Tilmes et al. (2012) climatology for 1995–2011, and the simulated ozone is averaged over our 2000–2010 simulation period. The locations of the sondes are shown in Figure S2 in the supporting information. The plots for individual sonde locations are labeled according to the regions defined in Tilmes et al. (2012) and Thompson et al. (2012). The simulated profiles show excellent agreement with the sondes, particularly for the equatorial America and Atlantic/Africa regions. Somewhat weaker agreement is seen for Hilo and Hong Kong, although the model still lies within the error bars (standard deviation) of the observations, and at Watukosek, where the simulated ozone does not capture the observed decrease with altitude in the upper troposphere. A similar comparison for January is provided in Figure S3 in the supporting information and shows good overall agreement between the observed and simulated profiles. The strong agreement between the observed and simulated profiles at most of the tropical sites suggests that the simulation captures important processes affecting the vertical structure of tropical ozone.

### 3.2. Ozone Under Clear Versus Cloudy Conditions

We next examine the simulated ozone profiles under clear versus cloudy conditions, as described in section 2.3. Figures 3 and 4 show the clear and cloudy ozone and carbon monoxide (CO) profiles averaged over several regions for January and July, respectively. The region boundaries are overplotted on the simulated July CO concentrations in Figure S2 in the supporting information. In January, the clear-sky ozone increases with altitude while the cloudy-sky ozone remains constant or

decreases with altitude between approximately 750 hPa and 400 hPa (Figures 3a–3c), consistent with the lofting of ozone-poor air from the surface during convection. The simulated ozone under cloudy conditions is systematically lower throughout the middle and upper troposphere than under clear-sky conditions. Similar features are seen in July (Figures 4a–4c), although the altitude range where cloudy-sky ozone is lower than clear-sky is smaller than for January.

We examine differences between polluted and clean regions using the simulated profiles of CO, a tracer of combustion produced by both fossil fuels and biomass burning. Previous studies have highlighted the influence of convection on the local vertical redistribution of CO (e.g., Marecal et al., 2006). Over the clean Southeast Pacific (Figures 3d and 4d), CO shows little variability with altitude and is nearly the same under clear versus cloudy conditions. In contrast, over the African continent (Figures 3e and 4e), CO peaks in the lower troposphere and CO in the free troposphere is elevated under cloudy conditions compared to clear-sky conditions, consistent with the upward transport of pollution by convection. The clear-sky versus cloudy-sky differences in simulated ozone and CO suggest that our simple criteria for defining clear versus cloudy grid boxes, despite ignoring the subgridscale differences in clouds, nevertheless produce physically meaningful separation between these two regimes.

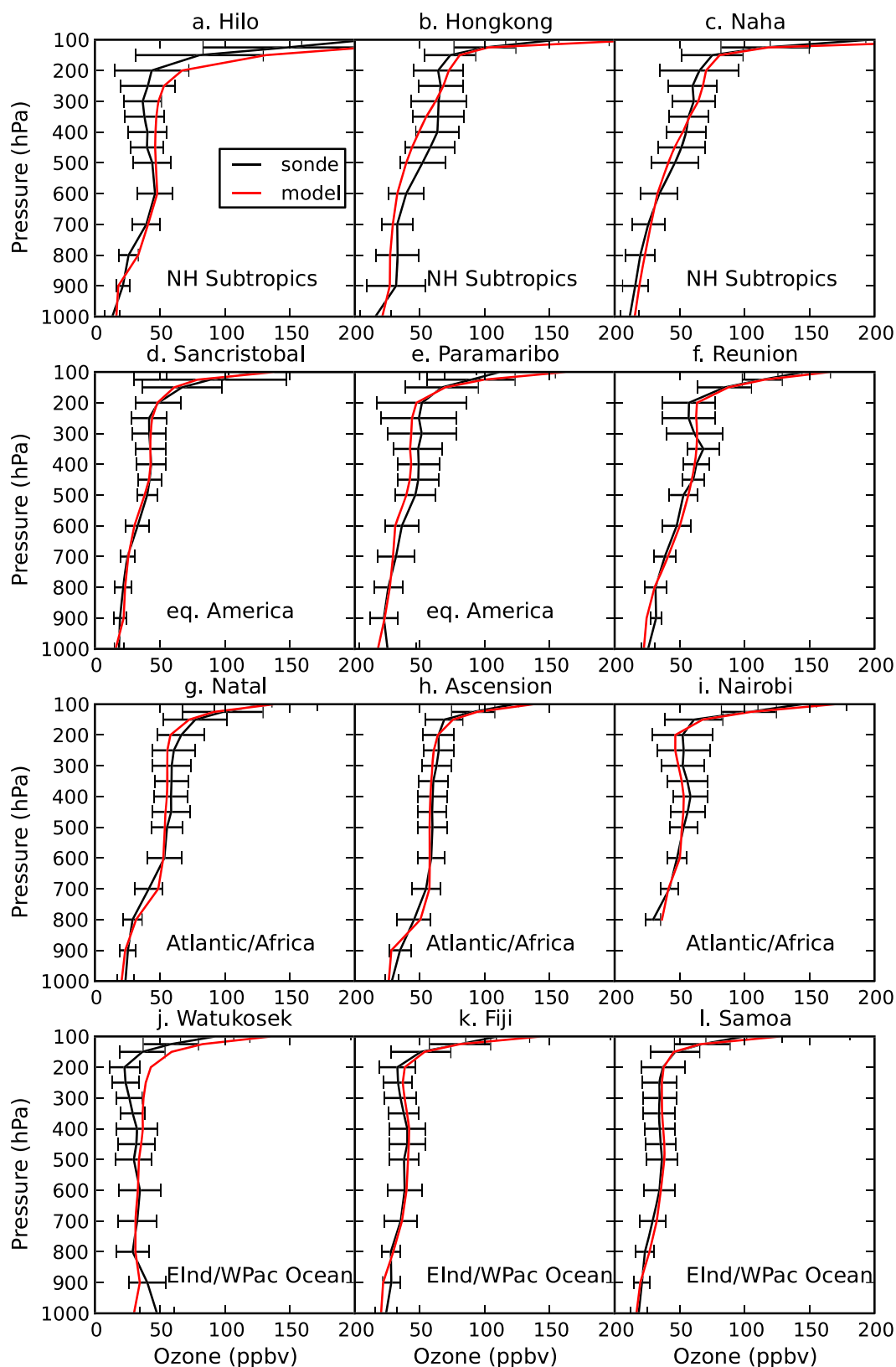


**Figure 2.** Simulated July ozone profiles averaged over 2000–2010 (red) compared to the July ozonesonde climatology (black) of Tilmes et al. (2012). The error bars represent the standard deviation of the sonde data. The text in the bottom right corner of each plot represents the region (if any) defined by Tilmes et al. (2012) and Thompson et al. (2012) to which the sonde belongs.

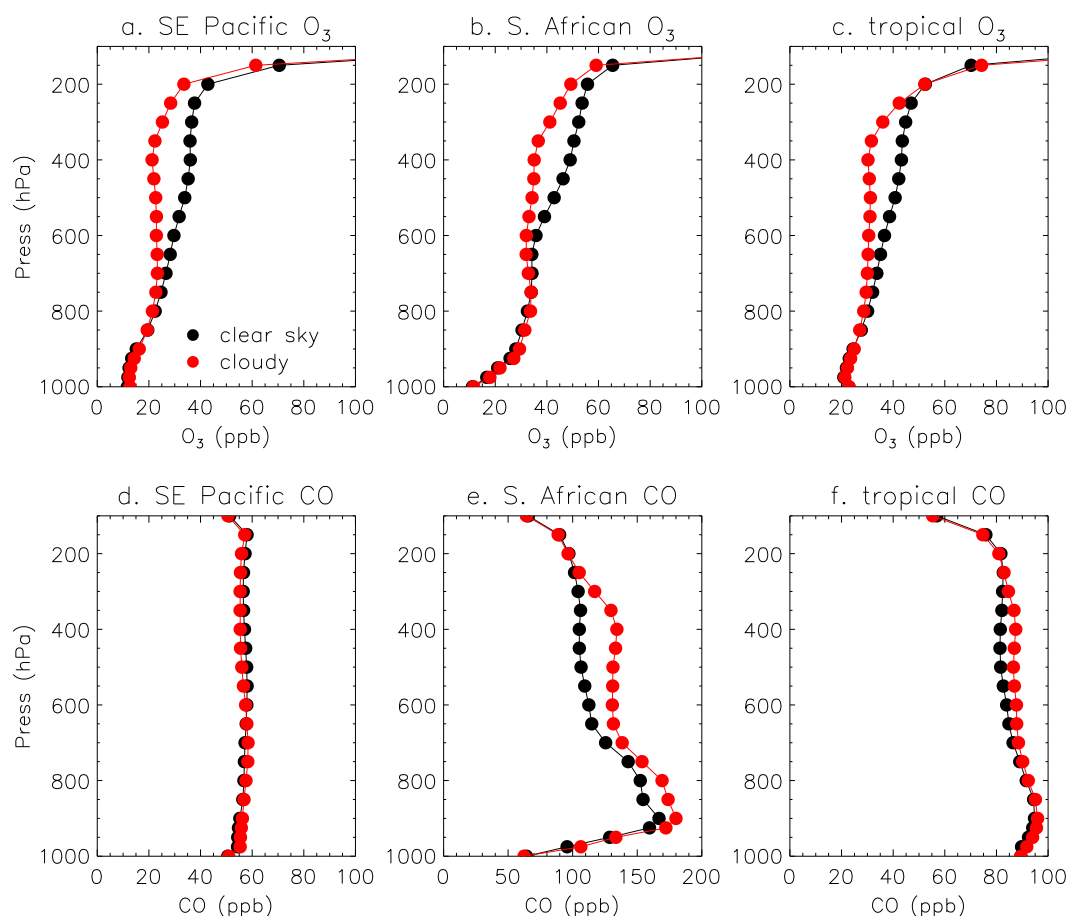


**Figure 3.** January (top row) simulated ozone and (bottom row) CO profiles averaged over the (a and d) Southeast Pacific (180°–120°W, 0°–30°S), (b and e) Southern Hemisphere Africa (10°E–40°E, 0°–30°S), and (c and f) the tropics (30°S–30°N) under cloudy (red) and clear-sky (black) conditions.

Ziemke et al. (2009) and Ziemke et al. (2017) noted that the OMI/MLS ozone shows elevated concentrations over Africa and South America compared to the Pacific in both cloud-free and deep convective cloud conditions. These features are evident in Figures 5a and 5b and 6a and 6b for January and July, respectively. We examine whether the simulated ozone under clear-sky and cloudy criteria reproduces the major features of the OMI/MLS geographic distribution. We plot model results for the 400 hPa level since this level shows a large separation between the clear-sky and cloudy-sky profiles in Figures 3 and 4.

In January, the 400 hPa simulated clear-sky ozone shows higher concentrations over Africa, eastern South America, and the Atlantic compared to the tropical Pacific, consistent with the background OMI/MLS observation (Figures 5a and 5c). It also captures the lower ozone at around 15°S compared to 5°S and 25°S over Africa. In the tropical grid boxes that both the OMI/MLS data and the simulation categorize as cloudy, the simulated January clear-sky ozone has a mean bias of 17% compared to OMI/MLS and a spatial correlation of  $r = 0.89$ .

The simulated cloudy-sky ozone shows similar geographic coverage and regions of missing data to the deep convective ozone observations (Figures 5b and 5d), indicating that the cloudy criterion successfully picks up much of the geographic distribution of deep convective clouds. After rebinning the model to the OMI/MLS resolution, we find that the model clear versus cloudy classification agrees with the OMI/MLS classification for 74% of tropical grid columns in January. The cloudy ozone is lower than the clear-sky ozone throughout the tropics in both the observations and the simulation. The simulated cloudy ozone captures the enhancement in ozone over equatorial Africa and the southern tip of Africa and in eastern South America seen in the deep convective observations, although it underestimates the magnitude of these enhancements partly due



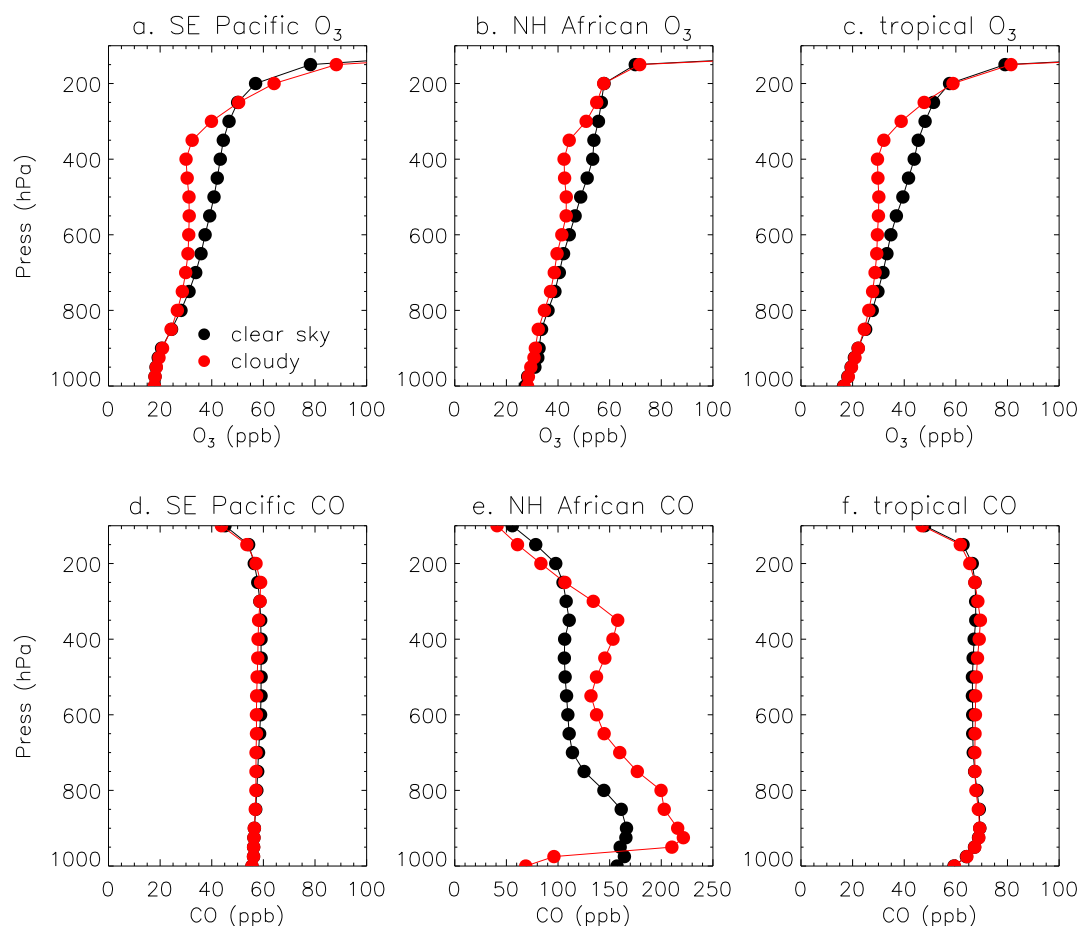


**Figure 4.** July (top row) simulated ozone and (bottom row) CO profiles averaged over the (a and d) Southeast Pacific (180°–120°W, 0°–30°S), (b and e) Northern Hemisphere Africa (10°W–40°E, 0°–30°N), and (c and f) the tropics (30°S–30°N) under cloudy (red) and clear-sky (black) conditions.

to lack of clouds in the simulation in the grid cells where the observed enhancements are largest. The ozone gradient between Africa and the Pacific is also less pronounced in the simulation than in the deep convective observations. The mean bias in simulated January tropical cloudy ozone is 11%, and the spatial correlation is  $r = 0.48$  for grid boxes that both the model and satellite data classify as cloudy.

While large differences in clear-sky versus cloudy-sky ozone are evident in the simulation at 400 hPa, almost no difference is seen at the surface (Figures 5e and 5f). This demonstrates that the differences seen at 400 hPa are due to differences in vertical transport and subsequent chemistry during convection rather than to differences in surface concentration.

In July (Figure 6), the simulated clear-sky ozone at 400 hPa reproduces the strong east-west gradient seen in the background observations, with high concentrations over equatorial Africa and the Atlantic and low concentrations over the West Pacific. However, the West Pacific concentrations in the simulation are not as low as in the observations. In the tropical grid boxes that both OMI/MLS and the simulation categorize as cloudy, the simulated July clear-sky ozone has a mean bias of 12% compared to OMI/MLS and a spatial correlation of  $r = 0.90$ .

The cloudy regions (those with data present) in the simulation are similar to the regions of data coverage in the deep convective observations, shifting from the Southern Hemisphere in January (Figure 5) to the Northern Hemisphere in July (Figure 6). Rebinning the model to the OMI/MLS resolution, we find that model classification of clear versus cloudy agrees with the OMI/MLS classification for 77% of the tropical grid columns in July. Both the simulated cloudy ozone at 400 hPa and the deep convective observations show enhancements over Africa compared to the surrounding oceans. The simulated cloudy ozone also shows

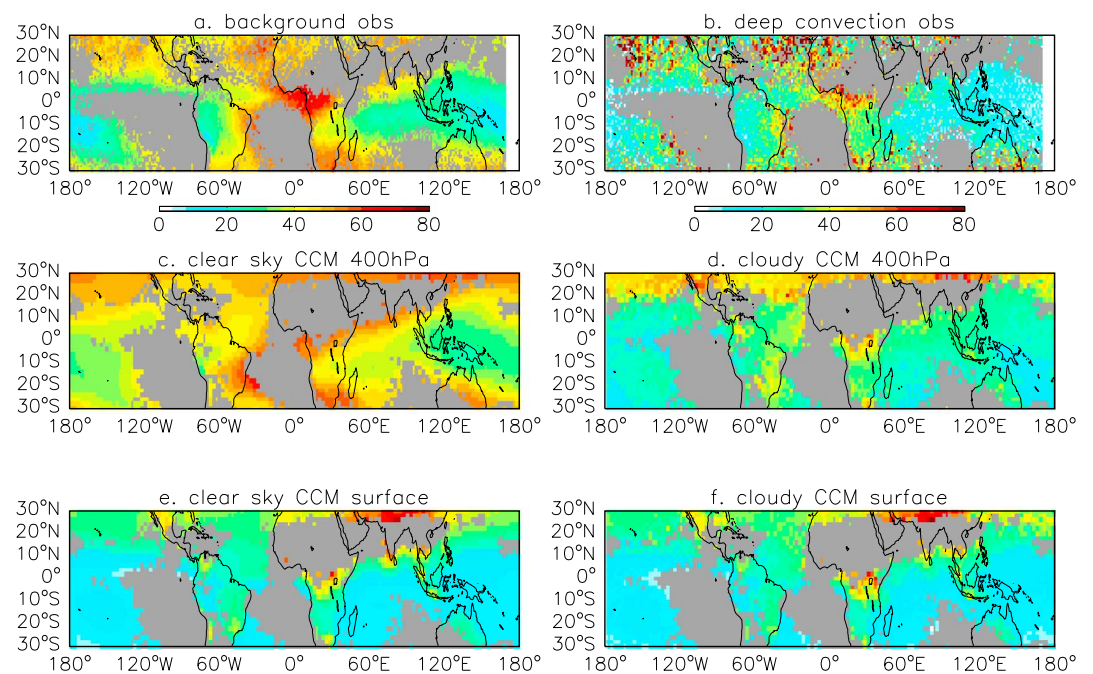


**Figure 5.** January ozone observations (ppbv) from the OMI/MLS residual method under (a) background and (b) deep convective conditions. Backgrounds versus deep convective conditions are defined in section 2.3. The gray areas indicate where deep convective data were unavailable, and these regions are grayed out in the background case as well for ease of comparison. January simulated ozone concentrations (in parts per billion) at 400 hPa for (c) clear-sky and (d) cloudy conditions, and at the surface for (e) clear-sky and (f) cloudy conditions. The gray areas indicate where no cloudy days were present, and these regions are grayed out in the clear-sky plots as well for ease of comparison.

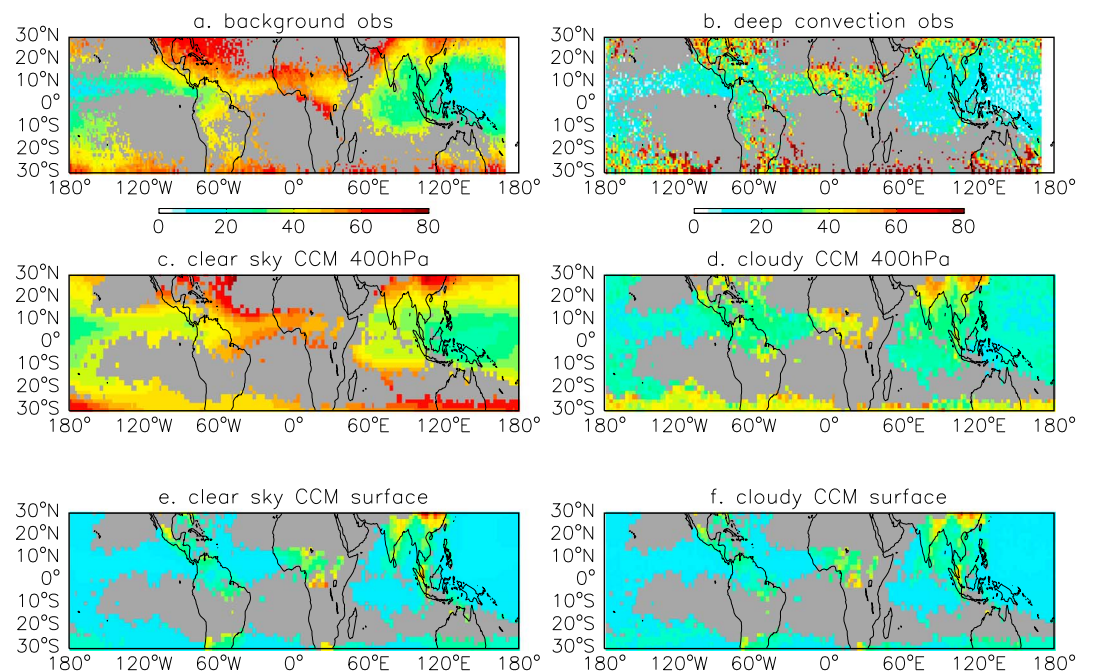


**Figure 6.** As in Figure 5, but for July. Concentrations are in parts per billion by volume.



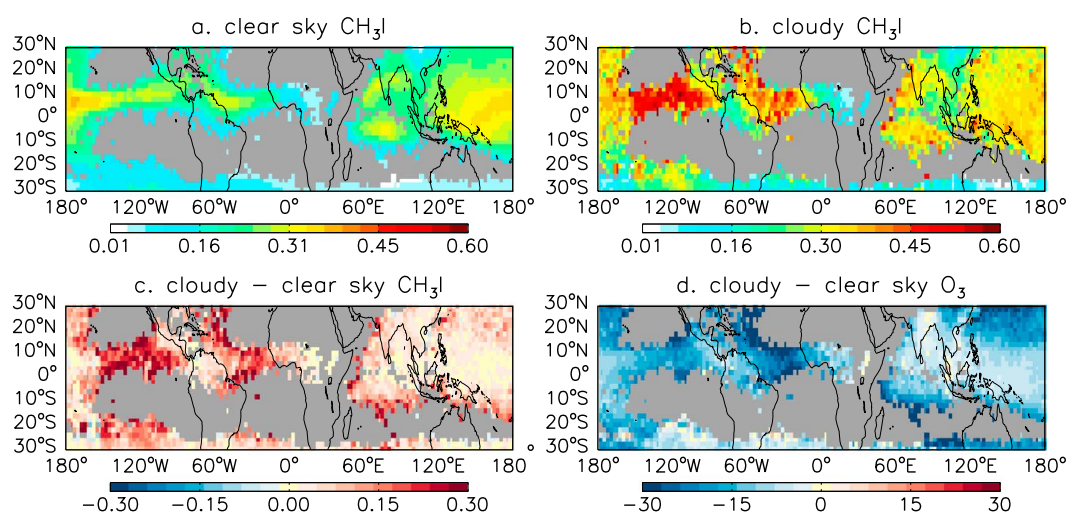


**Figure 7.** July 400 hPa concentrations of  $\text{CH}_3\text{I}$  (pptv) under (a) clear-sky and (b) cloudy conditions. The difference between cloudy and clear-sky conditions for (c)  $\text{CH}_3\text{I}$  (pptv) and (d)  $\text{O}_3$  (ppbv).

high values over the polluted regions of northeastern India and eastern China. While a hint of elevated values in these regions is visible in the deep convective observations, it is less pronounced than in the simulations, possibly due in part to noise in the data at the edge of the tropics. In the tropical grid boxes that both the satellite data and the simulation categorize as cloudy, the simulated July cloudy sky ozone has a mean bias of 6.1% compared to OMI/MLS and a spatial correlation of  $r = 0.51$ .

The integrated effect of differences in marine convection on clear versus cloudy days is evident in the simulated methyl iodide fields. Bell et al. (2002) demonstrated the utility of  $\text{CH}_3\text{I}$  for evaluating marine convection in global models. Figure 7 shows our simulated July  $\text{CH}_3\text{I}$  concentrations at 400 hPa for cloudy versus clear-sky conditions as well as the difference in simulated 400 hPa ozone in cloudy versus clear-sky conditions. Regions that show a large negative difference in cloudy compared to clear-sky ozone, such as the eastern Pacific and the Atlantic, also show large positive differences in  $\text{CH}_3\text{I}$ , indicating large enhancements in convection under cloudy versus clear-sky conditions in these regions.

### 3.3. Separating the Roles of Dynamics, Physics, and Chemistry

The geographic differences in both background and deep convective ozone observations suggest important differences in the relative importance of chemistry, convection, and large-scale transport between regions. We quantify the importance of these processes using model diagnostics for the ozone tendency due to dynamics (large-scale transport), physics (turbulence and convection), and chemistry. This analysis focuses on July, but similar results are obtained for January (Figure S4). Figure 8 shows the tendencies at 400 hPa for a single day in July and averaged over all July days between 2000 and 2010. For a single day, the ozone tendency is dominated by dynamics, which includes a noisy mix of positive and negative tendencies. The physics tendency is also important in some regions, while the chemistry tendency is relatively small.

The picture changes when we average over many July days (Figures 8b, 8d, and 8f). Coherent spatial patterns emerge in the dynamics tendency, which oppose the tendencies due to physics and/or chemistry. The tendency due to physics is large in regions with high convective mass flux (Figures 9a and 9b). It is primarily negative, representing the convective lifting of lower ozone air from below. However, the physics tendency is positive over the highly polluted regions in South and East Asia, where high ozone concentrations occur in the lower troposphere. The high pollution in these regions is evident in the elevated  $\text{NO}_2$  concentrations shown in Figures 9d and 9f. The ozone tendency due to chemistry is primarily positive at 400 hPa, indicating net ozone production. The positive tendency is particularly strong over the polluted regions of South and East Asia. Furthermore, the positive chemistry tendency over these regions is stronger on cloudy days than clear ones, as higher  $\text{NO}_2$  concentrations from convection and lightning are present on cloudy days (Figures 9c–9f).

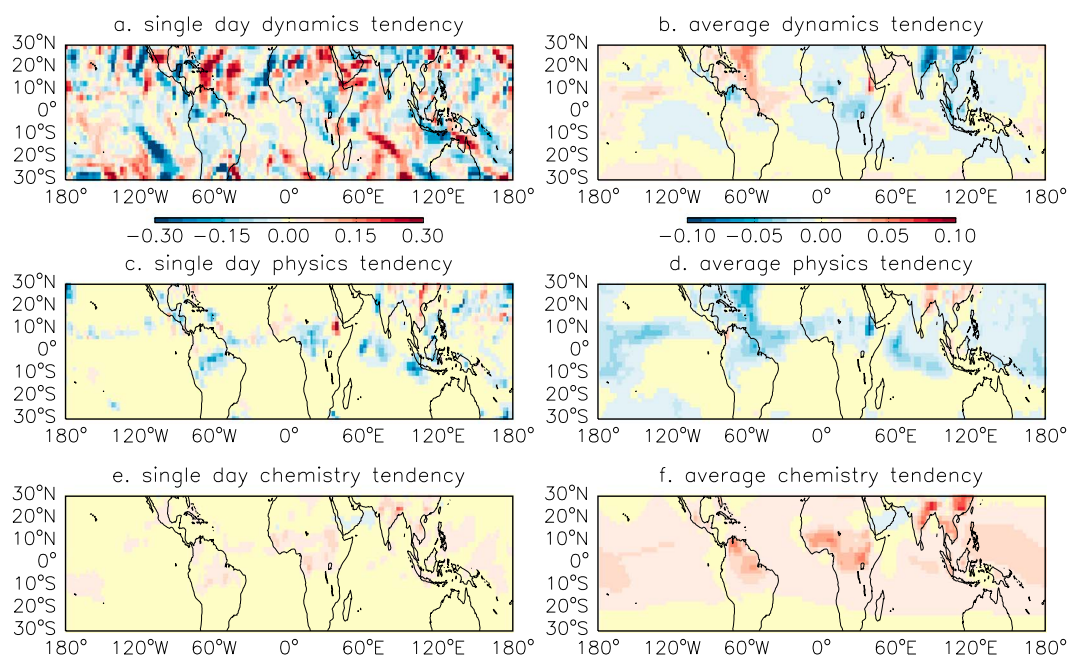


**Figure 8.** The tendency of ozone (ppt s<sup>-1</sup>) at 400 hPa due to (a and b) dynamics, (c and d) physics, and (e and f) chemistry for a single July day (Figures 8a, 8c, and 8e) and averaged over all July days from 2000 to 2010 (Figures 8b, 8d, and 8f).

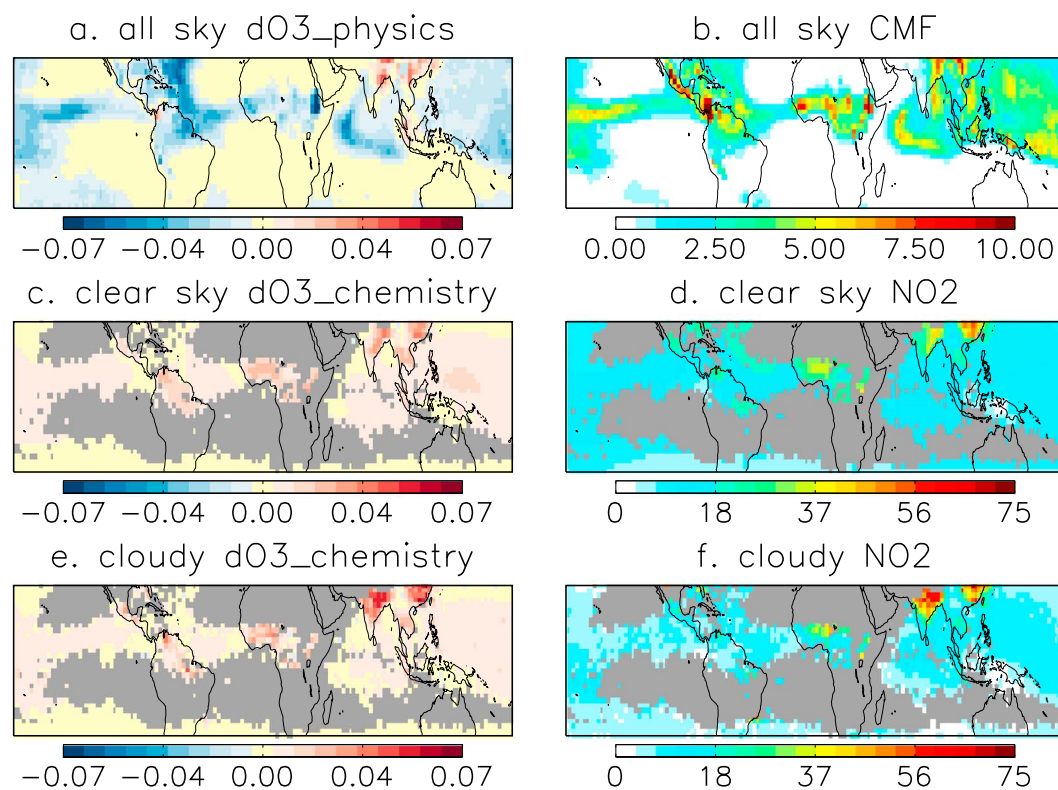


**Figure 9.** (a) The ozone tendency due to physics (ppt s<sup>-1</sup>) under both clear and cloudy conditions, (b) convective mass flux (g m<sup>-2</sup> s<sup>-1</sup>) under both clear and cloudy conditions, (c) ozone tendency due to chemistry (ppt s<sup>-1</sup>) under clear-sky conditions, (d) NO<sub>2</sub> concentrations (ppt) at the OMI overpass time under clear-sky conditions, (e) ozone tendency due to chemistry (ppt s<sup>-1</sup>) under cloudy conditions, and (f) NO<sub>2</sub> concentrations (ppt) at the OMI overpass time under cloudy conditions. All values are for 400 hPa and averaged over all Julys in the 2000–2010 simulation period.

Several factors influence the chemistry tendency at 400 hPa. As mentioned above, convective transport of ozone precursors and lightning  $\text{NO}_x$  production drive higher ozone production. On the other hand, wet deposition of  $\text{HNO}_3$  serves as a sink of  $\text{NO}_x$ , reducing ozone production. Deep convective clouds also alter photolysis frequencies, increasing  $J[\text{O}^1\text{D}]$  and  $J[\text{NO}_2]$  above the cloud and reducing it below (e.g., Liu et al., 2006). We find this effect in our analysis, which shows higher average values of  $J[\text{O}^1\text{D}]$  and  $J[\text{NO}_2]$  for cloudy grid boxes in the tropical upper troposphere and higher average values in clear boxes in the tropical lower troposphere. The switch from lower to higher cloud versus clear values occurs near the 400 hPa level shown in our analysis, and thus, the difference in the  $J[\text{O}^1\text{D}]$  and  $J[\text{NO}_2]$  photolysis frequencies for clear versus cloudy days, averaged over the tropics where cloudy results are available, is less than 2% at 400 hPa. The ozone tendency due to chemistry shown in Figures 8 and 9 represents the net effect of the multiple factors controlling ozone production and loss.

#### 4. Conclusions

Satellite observations of in-cloud ozone from OMI/MLS provide large-scale data on ozone concentrations in regions of deep-convective cloud. We demonstrate that a free-running CCM captures many of the differences between in-cloud and background ozone values seen in OMI/MLS observations. We develop a method that uses a threshold based on cloud fraction to determine “clear-sky” versus cloudy days. Using this method, we simulate the lower ozone values observed in cloudy conditions as well as spatial gradients between clean and polluted regions. The good agreement with observations suggests that the model represents well the impact of deep convection and clouds on ozone. Because this analysis technique does not depend on matching the cloud cover and meteorology of a specific day, it may be a valuable diagnostic for CCMs and model intercomparisons.

Stronger convection on cloudy days drives the differences between the simulated cloudy and clear-sky ozone concentrations in the middle troposphere. Simulated surface concentrations show little difference between cloudy and clear-sky days, indicating that the differences in the free troposphere are due to transport and the subsequent chemistry. While the ozone tendency due to convection is typically negative at the 400 hPa level, reflecting the transport of low ozone concentrations from the surface, the tendency is positive over the heavily polluted regions including parts of South and East Asia. Higher concentrations of ozone precursors aloft are also present during cloudy conditions in these regions, increasing the chemical production of ozone. By averaging over multiple years of simulation, we find coherent regional differences in the contributions of physics, chemistry, and large-scale dynamics to the 400 hPa ozone distribution of the tropical troposphere.

#### Acknowledgments

NASA's Modeling, Analysis, and Prediction program supported this work. Computer resources were provided by the NASA High-End Computing Program at the NASA Center for Climate Simulation. Output from the model simulation used in this study is included in the CCMI archive at the BADC (<http://blogs.reading.ac.uk/ccmi/badc-data-access/>). OMI/MLS in-cloud and background ozone data are available by request to Jerry Ziemke ([jerald.r.ziemke@nasa.gov](mailto:jerald.r.ziemke@nasa.gov)). The Tilmes et al. (2012) ozonesonde climatology was downloaded from <https://acom-staff.acom.ucar.edu/tilmes/ozone.html>.

#### References

- Bacmeister, J. T., Suarez, M. J., & Robertson, F. R. (2006). Rain reevaporation, boundary layer-convection interactions, and Pacific rainfall patterns in a AGCM. *Journal of the Atmospheric Sciences*, 63(12), 3383–3403. <https://doi.org/10.1175/JAS3791.1>
- Bell, N., Hsu, L., Jacob, D., Schultz, M., Blake, D., Butler, J., ... Maier-Reimer, E. (2002). Methyl iodide: Atmospheric budget and use as a tracer of marine convection in global models. *Journal of Geophysical Research*, 107(D17), ACH 8-1–ACH 8-12. <https://doi.org/10.1029/2001JD001151>
- Bertram, T., Perring, A., Wooldridge, P. J., Crounse, J. D., Kwan, A. J., Wennberg, P., ... Cohen, R. C. (2007). Direct measurements of the convective recycling of the upper troposphere. *Science*, 315(5813), 816–820. <https://doi.org/10.1126/science.1134548>
- Bowman, K. W., Shindell, D. T., Worden, H. M., Lamarque, J. F., Young, P. J., Stevenson, D. S., ... Worden, J. R. (2013). Evaluation of ACCMIP outgoing longwave radiation from tropospheric ozone using TES satellite observations. *Atmospheric Chemistry and Physics*, 13(8), 4057–4072. <https://doi.org/10.5194/acp-13-4057-2013>
- Chin, M., Shindell, D. T., Worden, H. M., Lamarque, J. F., Young, P. J., Stevenson, D. S., ... Worden, J. R. (2002). Tropospheric aerosol optical thickness from the GOCART model and comparisons with satellite and Sun photometer measurements. *Journal of the Atmospheric Sciences*, 59(3), 461–483. [https://doi.org/10.1175/1520-0469\(2002\)059%3C0461:TAOTFT%3E2.0.CO;2](https://doi.org/10.1175/1520-0469(2002)059%3C0461:TAOTFT%3E2.0.CO;2)
- Colarco, P., da Silva, A., Chin, M., & Diehl, T. (2010). Online simulations of global aerosol distributions in the NASA GEOS-4 model and comparisons to satellite and ground-based aerosol optical depth. *Journal of Geophysical Research*, 115(D14), D14207. <https://doi.org/10.1029/2009JD012820>
- Duncan, B. N., Strahan, S. E., Yoshida, Y., Steenrod, S. D., & Livesey, N. (2007). Model study of the cross-tropopause transport of biomass burning pollution. *Atmospheric Chemistry and Physics*, 7(14), 3713–3736. <https://doi.org/10.5194/acp-7-3713-2007>
- Eyring, V., Lamarque, J.-F., Hess, P., Arfeuille, F., Bowman, K., Chipperfield, M. P., ... Giorgetta, M. A. (2013). Overview of IGAC/SPARC Chemistry-Climate Model Initiative (CCMI) community simulations in support of upcoming ozone and climate assessments. *Spac Newsletter*, 40, 48–66.
- Fishman, J., & Larsen, J. (1987). Distribution of total ozone and stratospheric ozone in the tropics—Implications for the distribution of tropospheric ozone. *Journal of Geophysical Research*, 92(D6), 6627–6634. <https://doi.org/10.1029/JD092iD06p06627>
- Folkens, I., Braun, C., Thompson, A., & Witte, J. (2002). Tropical ozone as an indicator of deep convection. *Journal of Geophysical Research*, 107(D13), ACH 13-1–ACH 13-10. <https://doi.org/10.1029/2001JD001178>



- Gidel, L. (1983). Cumulus cloud transport of transient tracers. *Journal of Geophysical Research*, 88(C11), 6587–6599. <https://doi.org/10.1029/JC088iC11p06587>
- Granier, C., Bessagnet, B., Bond, T., D'Angiola, A., van der Gon, H. D., Frost, G. J., ... van Vuuren, D. P. (2011). Evolution of anthropogenic and biomass burning emissions of air pollutants at global and regional scales during the 1980–2010 period. *Climatic Change*, 109(1–2), 163–190. <https://doi.org/10.1007/s10584-011-0154-1>
- Helfand, H. M., & Schubert, S. D. (1995). Climatology of the simulated Great Plains low-level jet and its contribution to the continental moisture budget of the United States. *Journal of Climate*, 8(4), 784–806. [https://doi.org/10.1175/1520-0442\(1995\)008%3C0784:COTSGP%3E2.0.CO;2](https://doi.org/10.1175/1520-0442(1995)008%3C0784:COTSGP%3E2.0.CO;2)
- Huntrieser, H., Lichtenstern, M., Scheibe, M., Aufmhoff, H., Schlager, H., Pucik, T., ... Barth, M. C. (2016). On the origin of pronounced O<sub>3</sub> gradients in the thunderstorm outflow region during DC3. *Journal of Geophysical Research: Atmospheres*, 121(11), 6600–6637. <https://doi.org/10.1002/2015JD024279>
- Jacob, D. J. (2000). Heterogeneous chemistry and tropospheric ozone. *Atmospheric Environment*, 34(12–14), 2131–2159. [https://doi.org/10.1016/S1352-2310\(99\)00462-8](https://doi.org/10.1016/S1352-2310(99)00462-8)
- Joiner, J., Schoeberl, M. R., Vasilkov, A. P., Oreopoulos, L., Platnick, S., Livesey, N. J., & Levelt, P. F. (2009). Accurate satellite-derived estimates of the tropospheric ozone impact on the global radiation budget. *Atmospheric Chemistry and Physics*, 9(13), 4447–4465. <https://doi.org/10.5194/acp-9-4447-2009>
- Joiner, J., Vasilkov, A. P., Gupta, P., Bhartia, P. K., Veefkind, P., Sneep, M., ... Spurr, R. (2012). Fast simulators for satellite cloud optical centroid pressure retrievals; evaluation of OMI cloud retrievals. *Atmospheric Measurement Techniques*, 5(3), 529–545. <https://doi.org/10.5194/amt-5-529-2012>
- Kley, D., Crutzen, P., Smit, H., Vomel, H., Oltmans, S., Grassl, H., & Ramanathan, V. (1996). Observations of near-zero ozone concentrations over the convective Pacific: Effects on air chemistry. *Science*, 274(5285), 230–233. <https://doi.org/10.1126/science.274.5285.230>
- Lacis, A., Wuebbles, D., & Logan, J. (1990). Radiative forcing of climate by changes in the vertical distribution of ozone. *Journal of Geophysical Research*, 95(D7), 9971–9981. <https://doi.org/10.1029/JD095iD07p09971>
- Lamarque, J. F., Shindell, D. T., Josse, B., Young, P. J., Cionni, I., Eyring, V., ... Zeng, G. (2013). The Atmospheric Chemistry and Climate Model Intercomparison Project (ACCMIP): Overview and description of models, simulations and climate diagnostics. *Geoscientific Model Development*, 6(1), 179–206. <https://doi.org/10.5194/gmd-6-179-2013>
- Lang, C., Waugh, D., Olsen, M., Douglass, A., Liang, Q., Nielsen, J., ... Stolarski, R. (2012). The impact of greenhouse gases on past changes in tropospheric ozone. *Journal of Geophysical Research*, 117, D23304. <https://doi.org/10.1029/2012JD018293>
- Lawrence, M. G., von Kuhlmann, R., Salzmann, M., & Rasch, P. J. (2003). The balance of effects of deep convective mixing on tropospheric ozone. *Geophysical Research Letters*, 30(18), 1940. <https://doi.org/10.1029/2003GL017644>
- Lelieveld, J., & Crutzen, P. (1994). Role of deep cloud convection in the ozone budget of the troposphere. *Science*, 264(5166), 1759–1761. <https://doi.org/10.1126/science.264.5166.1759>
- Liaskos, C., Allen, D., & Pickering, K. (2015). Sensitivity of tropical tropospheric composition to lightning NO<sub>x</sub> production as determined by replay simulations with GEOS-5. *Journal of Geophysical Research: Atmospheres*, 120(16), 8512–8534. <https://doi.org/10.1002/2014JD022987>
- Liu, H., Crawford, J. H., Pierce, R. B., Norris, P., Platnick, S. E., Chen, G., ... Tie, X. (2006). Radiative effect of clouds on tropospheric chemistry in a global three-dimensional chemical transport model. *Journal of Geophysical Research*, 111(D20), D20303. <https://doi.org/10.1029/2005JD06403>
- Lock, A. P., Brown, A. R., Bush, M. R., Martin, G. M., & Smith, R. N. B. (2000). A new boundary layer mixing scheme. Part I: Scheme description and single-column model tests. *Monthly Weather Review*, 128, 3187–3199.
- Louis, J. F., & Geleyn, J. (1982). A short history of the PBL parameterization at ECMWF. In *Proceeding ECMWF Workshop on Planetary Boundary Layer Parameterization* (pp. 59–80). Reading, United Kingdom: ECMWF.
- Marecal, V., Riviere, E., Held, G., Cautenet, S., & Freitas, S. (2006). Modelling study of the impact of deep convection on the utls air composition—Part I: Analysis of ozone precursors. *Atmospheric Chemistry and Physics*, 6(6), 1567–1584. <https://doi.org/10.5194/acp-6-1567-2006>
- Molod, A., Takacs, L., Suarez, M., & Bacmeister, J. (2015). Development of the GEOS-5 atmospheric general circulation model: Evolution from MERRA to MERRA2. *Geoscientific Model Development*, 8(5), 1339–1356. <https://doi.org/10.5194/gmd-8-1339-2015>
- Moorthi, S., & Suarez, M. J. (1992). Relaxed Arakawa Schubert: A parameterization of moist convection for general circulation models. *Monthly Weather Review*, 120(6), 978–1002. [https://doi.org/10.1175/1520-0493\(1992\)120%3C0978:RASAPD%3E2.0.CO;2](https://doi.org/10.1175/1520-0493(1992)120%3C0978:RASAPD%3E2.0.CO;2)
- Morgenstern, O., Hegglin, M. I., Rozanov, E., O'Connor, F. M., Abraham, N. L., Akiyoshi, H., ... Zeng, G. (2017). Review of the global models used within phase 1 of the Chemistry–Climate Model Initiative (CCMI). *Geoscientific Model Development*, 10(2), 639–671. <https://doi.org/10.5194/gmd-10-639-2017>
- Oman, L., Douglass, A., Ziemke, J., Rodriguez, J., Waugh, D., & Nielsen, J. (2013). The ozone response to ENSO in Aura satellite measurements and a chemistry–climate simulation. *Journal of Geophysical Research: Atmospheres*, 118(2), 965–976. <https://doi.org/10.1029/2012JD018546>
- Oman, L. D., Ziemke, J. R., Douglass, A. R., Waugh, D. W., Lang, C., Rodriguez, J. M., & Nielsen, J. E. (2011). The response of tropical tropospheric ozone to ENSO. *Geophysical Research Letters*, 38(13), L13706. <https://doi.org/10.1029/2011GL047865>
- Pan, L., Honomichl, S. B., Randel, W. J., Apel, E. C., Atlas, E. L., Beaton, S. P., ... Weinheimer, A. J. (2015). Bimodal distribution of free tropospheric ozone over the tropical western Pacific revealed by airborne observations. *Geophysical Research Letters*, 42(18), 7844–7851. <https://doi.org/10.1002/2015GL065562>
- Pawson, S., Stolarski, R., Douglass, A., Newman, P., Nielsen, J., Frith, S., & Gupta, M. (2008). Goddard Earth Observing System chemistry–climate model simulations of stratospheric ozone–temperature coupling between 1950 and 2005. *Journal of Geophysical Research*, 113(D12), D12103. <https://doi.org/10.1029/2007JD009511>
- Pickering, K., Thompson, A., Scala, J., Tao, W., Dickerson, R., & Simpson, J. (1992). Free tropospheric ozone production following entrainment of urban plumes into deep convection. *Journal of Geophysical Research*, 97(D16), 17,985–18,000. <https://doi.org/10.1029/92JD01716>
- Rayner, N., Parker, D., Horton, E., Folland, C., Alexander, L., Rowell, D., ... Kaplan, A. (2003). Global analyses of sea surface temperature, sea ice, and night marine air temperature since the late nineteenth century. *Journal of Geophysical Research*, 108(D14), 4407. <https://doi.org/10.1029/2002JD002670>
- Solomon, S., Thompson, D., Portmann, R., Oltmans, S., & Thompson, A. (2005). On the distribution and variability of ozone in the tropical upper troposphere: Implications for tropical deep convection and chemical–dynamical coupling. *Geophysical Research Letters*, 32(23), L23813. <https://doi.org/10.1029/2005GL024323>
- Stajner, I., Wargan, K., Pawson, S., Hayashi, H., Chang, L.-P., Hudman, R. C., ... Witte, J. C. (2008). Assimilated ozone from EOS-Aura: Evaluation of the tropopause region and tropospheric columns. *Journal of Geophysical Research*, 113(D16), D16532. <https://doi.org/10.1029/2007JD008863>

- Stammes, P., Snee, M., de Haan, J. F., Veefkind, J. P., Wang, P., & Levelt, P. F. (2008). Effective cloud fractions from the Ozone Monitoring Instrument: Theoretical framework and validation. *Journal of Geophysical Research*, 113(D16), D16538. <https://doi.org/10.1029/2007JD008820>
- Strahan, S. E., Duncan, B. N., & Hoor, P. (2007). Observationally derived transport diagnostics for the lowermost stratosphere and their application to the GMI chemistry and transport model. *Atmospheric Chemistry and Physics*, 7(9), 2435–2445. <https://doi.org/10.5194/acp-7-2435-2007>
- Thompson, A., Miller, S. K., Tilmes, S., Kollonige, D. W., Witte, J. C., Oltmans, S. J., ... Thuy Ha, H. T. (2012). Southern Hemisphere Additional Ozone sondes (SHADOZ) ozone climatology (2005–2009): Tropospheric and tropical tropopause layer (TTL) profiles with comparisons to OMI-based ozone products. *Journal of Geophysical Research*, 117(D23), D23301. <https://doi.org/10.1029/2011JD016911>
- Thompson, A., Oltmans, S., Tarasick, D., von der Gathen, P., Smit, H., & Witte, J. (2011). Strategic ozone sounding networks: Review of design and accomplishments. *Atmospheric Environment*, 45(13), 2145–2163. <https://doi.org/10.1016/j.atmosenv.2010.05.002>
- Thompson, A., Tao, W., Pickering, K., Scala, J., & Simpson, J. (1997). Tropical deep convection and ozone formation. *Bulletin of the American Meteorological Society*, 78(6), 1043–1054. [https://doi.org/10.1175/1520-0477\(1997\)078%3C1043:TDCAOF%3E2.0.CO;2](https://doi.org/10.1175/1520-0477(1997)078%3C1043:TDCAOF%3E2.0.CO;2)
- Thompson, A., Witte, J. C., Oltmans, S. J., Schmidlin, F. J., Logan, J. A., Fujiwara, M., ... Kelder, H. M. (2003). Southern Hemisphere Additional Ozone sondes (SHADOZ) 1998–2000 tropical ozone climatology—2. Tropospheric variability and the zonal wave-one. *Journal of Geophysical Research*, 108(D2), 8241. <https://doi.org/10.1029/2002JD002241>
- Tilmes, S., Lamarque, J.-F., Emmons, L. K., Conley, A., Schultz, M. G., Saunio, M., ... Tarasick, D. (2012). Technical note: Ozone sonde climatology between 1995 and 2011: Description, evaluation and applications. *Atmospheric Chemistry and Physics*, 12(16), 7475–7497. <https://doi.org/10.5194/acp-12-7475-2012>
- Vasilkov, A., Joiner, J., Spurr, R., Bhartia, P., Levelt, P., & Stephens, G. (2008). Evaluation of the OMI cloud pressures derived from rotational Raman scattering by comparisons with other satellite data and radiative transfer simulations. *Journal of Geophysical Research*, 113, D15S19. <https://doi.org/10.1029/2007JD008689>
- Voulgarakis, A., Wild, O., Savage, N. H., Carver, G. D., & Pyle, J. A. (2009). Clouds, photolysis, and regional tropospheric ozone budgets. *Atmospheric Chemistry and Physics*, 9(21), 8235–8246. <https://doi.org/10.5194/acp-9-8235-2009>
- Wang, C., & Prinn, R. (2000). On the roles of deep convective clouds in tropospheric chemistry. *Journal of Geophysical Research*, 105(D17), 22,269–22,297. <https://doi.org/10.1029/2000JD900263>
- Ziemke, J., Chandra, S., Duncan, B., Froidevaux, L., Bhartia, P., Levelt, P., & Waters, J. (2006). Tropospheric ozone determined from aura OMI and MLS: Evaluation of measurements and comparison with the Global Modeling Initiative's Chemical Transport Model. *Journal of Geophysical Research*, 111(D19), D19303. <https://doi.org/10.1029/2006JD007089>
- Ziemke, J., Douglass, A., Oman, L., Strahan, S., & Duncan, B. (2015). Tropospheric ozone variability in the tropics from ENSO to MJO and shorter timescales. *Atmospheric Chemistry and Physics*, 15(14), 8037–8049. <https://doi.org/10.5194/acp-15-8037-2015>
- Ziemke, J., Joiner, J., Chandra, S., Bhartia, P., Vasilkov, A., Haffner, D., ... Levelt, P. (2009). Ozone mixing ratios inside tropical deep convective clouds from OMI satellite measurements. *Atmospheric Chemistry and Physics*, 9(2), 573–583. <https://doi.org/10.5194/acp-9-573-2009>
- Ziemke, J. R., Chandra, S., Labow, G. J., Bhartia, P. K., Froidevaux, L., & Witte, J. C. (2011). A global climatology of tropospheric and stratospheric ozone derived from Aura OMI and MLS measurements. *Atmospheric Chemistry and Physics*, 11(17), 9237–9251. <https://doi.org/10.5194/acp-11-9237-2011>
- Ziemke, J. R., Strode, S. A., Douglass, A. R., Joiner, J., Vasilkov, A., Oman, L. D., ... Haffner, D. P. (2017). A cloud-ozone data product from Aura OMI and MLS satellite measurements. *Atmospheric Measurement Techniques Discussions*, 1–29. <https://doi.org/10.5194/amt-2017-107>
- Ziemke, J. R., Chandra, S., & Bhartia, P. K. (2001). Cloud slicing: A new technique to derive upper tropospheric ozone from satellite measurements. *Journal of Geophysical Research*, 106(D9), 9853–9867. <https://doi.org/10.1029/2000JD900768>